Tomographic inversions from the Fram Strait 2008-9 experiment

E. Skarsoulis,[1] G. Piperakis,[1] M. Kalogerakis,[2,1] H. Sagen,[3] S. Haugen,[3]
A. Beszczynska-Möller,[4] P. Worcester[5]

[1]Institute of Applied and Computational Mathematics, Foundation for Research and Technology Hellas,
PO Box 1527, 711 10 Heraklion, Crete, Greece, {**eskars, piperak, mixalis**}**@iacm.forth.gr**
[2]Technological Education Institute-Crete, PO Box 1939, 710 04 Heraklion, Crete, Greece
[3]Nansen Environmental and Remote Sensing Center, Thormøhlensgt 47, 5006 Bergen, Norway,
hanne.sagen@nersc.no, sah@sahaugen.no
[4]Alfred Wegener Institute for Polar and Marine Research, Postfach 12 01 61, 27515 Bremerhaven,
Germany, **Agnieszka.Beszczynska-Moeller@awi.de**
[5]Scripps Institution of Oceanography, University of California, San Diego, 9500 Gilman Drive,
0225, La Jolla, CA 92093-0225, USA, **pworcester@ucsd.edu**

The Fram Strait is the main passage through which mass and heat exchange between the Atlantic and Arctic Ocean takes place. A tomography experiment was conducted from September 2008 to August 2009 in the eastern Fram Strait in the framework of the DAMOCLES EU/FP6 project. The experiment involved an acoustic source west of Spitzbergen and a vertical receiving array in the middle of the strait. The one-year long series of travel-time data from the vertical receiving array are analysed to recover temperature variations along the 130-km section over the duration of the experiment. The temperature distribution is parameterized in terms of empirical orthogonal functions (EOFs) based on historical data. A Markov Chain Monte Carlo (MCMC) inversion scheme is used relying on the matched-peak approach, seeking to maximize the agreement between theoretical and measured travel times.

1   Introduction

The deep and wide Fram Strait, between Greenland and Spitzbergen, is the main passage through which the mass and heat exchange between the Atlantic and Arctic Ocean takes place: on the eastern side of the strait the northward West Spitzbergen Current (WSC) brings Atlantic water to the Arctic Ocean whereas on the western side the southward East Greenland Current (EGC) brings cold water and ice from the Arctic back to the Atlantic ocean. Between these two current systems the Return Atlantic Current (RAC) recirculates water masses from the western flank of the WSC back into the Atlantic (see Fig. 1). The RAC is responsible to a large extent for the variability in the heat flux through the strait [1].

A 10-month long tomography experiment was conducted from 21 September 2008 until 31 July 2009 in the framework of DAMOCLES EU/FP6 project to monitor the average heat content along a 130-km transect across the eastern part of the Fram Strait and contribute to improved estimation of heat fluxes through the strait by assimilation in fine-scale oceanographic models. The experiment involved a sweep-frequency source (S in Fig. 1) at 78º30.6'N, 8º15.1'E, at a depth of 378 m, and a vertical receiver array (R in Fig. 1) at 78º25.5'N, 2º26.5'E with 8 hydrophones spanning the depths between 295 m and 973 m. The source-receiver range corresponding to the above locations is 130.01 km. The source emitted 60s long sweeps every 3 hours between 190 and 290 Hz at a level of 190 dB re 1µPa@1m. The receiver array was setup by combining two extended STAR arrays (4 hydrophones each) in a tail to tail configuration [2], [3].
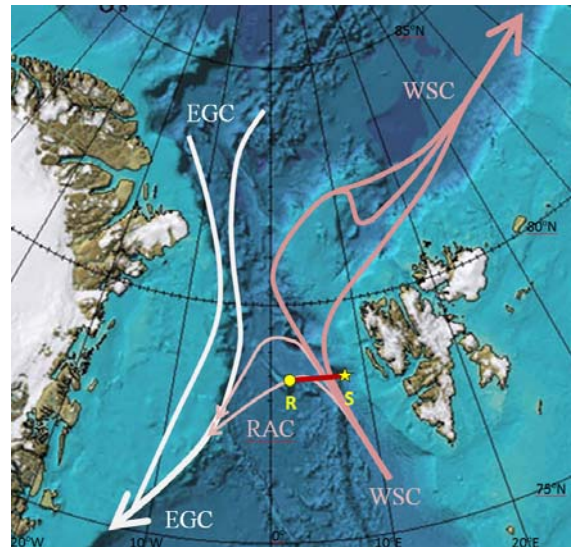

Fig. 1. Experiment area, source (S), receiver (R) location.

Short baseline systems were used to monitor mooring motion and correct for displacements of the source and the receiver during the experiment. In the case of the receiver the short baseline system monitored the position of the two STAR control units at the upper and lower part of the array (at 295 m and 973 m, respectively) and the correction for each hydrophone was estimated by interpolation.

2   Parameterization

The temperature distribution $T(r,z)$ on the vertical plane between source and receiver, as a function of range (r) and depth (z), can be parameterized as a modal sum

$$T(r,z) = T_0(r,z) + \sum_{\ell}^{L} \vartheta_\ell f_\ell(r,z)$$

where $T_0(r,z)$ is the background (reference) temperature distribution, $f_\ell(r,z)$ are the temperature modes (e.g. empirical orthogonal functions - EOFs) and ϑ_ℓ are the modal amplitudes. The parameterization for the Fram Strait experiment relies on EOF analysis of moored-array data collected by the Alfred Wegener Institute (AWI) in the period from January 2006 to June 2008 along $78^o50'$N.
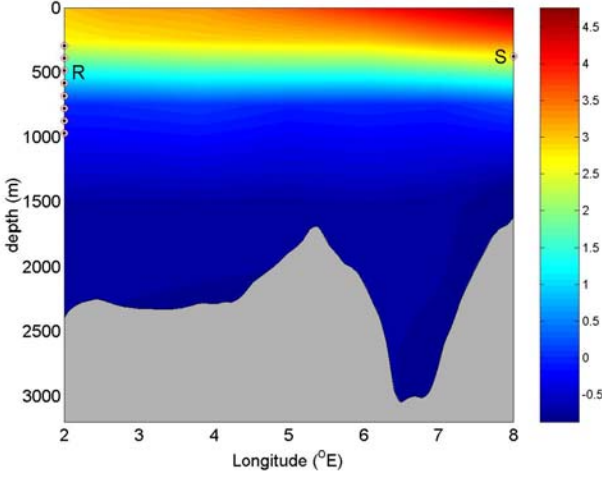

Fig. 2. Mean temperature distribution along the tomography section and location of source (S) and receiving hydrophones (R).

Fig. 2 shows the average temperature distribution from the AWI moored-array data. The basic thermocline reaching 500 m depth and the warm-water signature of the West Spitzbergen current on the east are clearly seen in this figure. Fig. 3 shows the first 6 temperature EOFs as functions of range and depth explaining 91% of the observed variance; the rms amplitudes are 2.4, 0.8, 0.8, 0.7, 0.5 and 0.4 respectively. EOF-1 accounts for the bulk of the seasonal variability which takes place close to the surface. Higher-order EOFs penetrate into deeper layers describing horizontal and vertical modes of variability.

The Chen-Millero formula [4] is used to convert temperature distributions into sound-speed distributions assuming a constant salinity of 35 ppt, which is an average value for the salinity in the area.

3   Model relations

On the basis of the previous parameterization the vector $\vec{\vartheta} = \{\vartheta_1, \vartheta_2, \ldots, \vartheta_L\}$ of EOF amplitudes describes a model state, i.e. a possible temperature distribution. The set of acceptable model states are described by the parameter space Θ in which the vector $\vec{\vartheta}$ belongs; the rms amplitudes of the EOFs give valuable information for the construction/constraining of Θ.
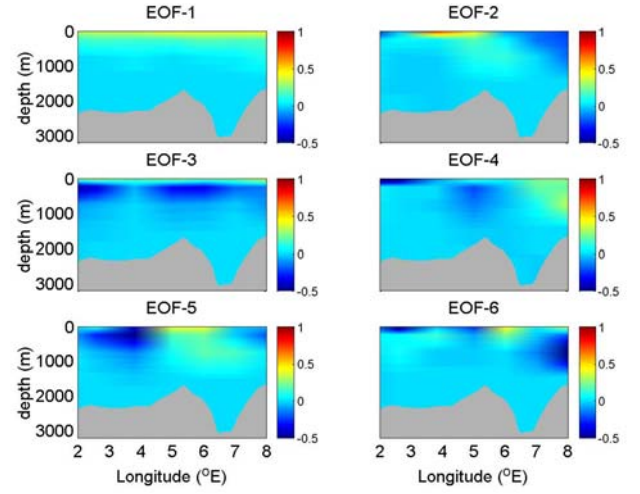

Fig. 3. The first 6 temperature EOFs.

Using the temperature parameterization and temperature-to-sound-speed conversion and performing acoustic propagation calculations (assuming fixed source and receiver positions) a mapping g_i from model states $\vec{\vartheta}$ to travel times τ_i can be obtained.

$$\tau_i = g_i(\vec{\vartheta}), \quad i = 1, \ldots, I(\vec{\vartheta}), \quad \vec{\vartheta} \in \Theta ,$$

The number I is the number of arrivals corresponding to the model state $\vec{\vartheta}$.

In the case of a vertical receiving array the model relations can be extended to cover time and depth (at the given range)

$$\tau = g(\varphi; \vec{\vartheta}), \quad z = h(\varphi; \vec{\vartheta}), \quad \vec{\vartheta} \in \Theta ,$$

where φ is the launch angle at the source, which is used as a parametric description of the time/depth arrivals. The time-depth curves are continuous curves in the time-depth domain. The discrete travel times correspond to the roots of the equation $z_R = h(\varphi)$, where z_R is the depth of the single receiver.

4   Matched-peak inversion

The matched-peak solution to the inversion problem consists in finding the population of model states that interpret (identify) the maximum number of peaks in each reception [5]. For this purpose the parameter domain is discretized into a finite set of model states. The discrete model states may either lie on a regular grid or have a random distribution. Using the model relations, arrival times are predicted for each model state and compared with the observed ones seeking to maximize the number of matches.

The discrete model states are denoted by $\vec{\vartheta}_k$, $k = 1, \ldots, K$ where the index k spans the parameter domain Θ. The

model relations can be used to calculate the arrival times corresponding to the discrete model states.

$$\tau_{i,k} = g_i\left(\vec{\vartheta}_k\right), \quad i = 1,\dots,I(\vec{\vartheta}_k), \quad k = 1,\dots,K$$

Due to the discrete coverage of the parameter domain certain tolerances have to be accounted for when looking for associations between model arrivals and observed peaks. Apart from this the predicted arrival times are also subject to modeling errors, whereas the arrival-time observation is subject to an error as well. The cumulative discretization, modeling and observation error, denoted by ε_i, is the total tolerance that has to be allowed for when matching the predicted arrival times, corresponding to the discrete model states, with observed travel-time data.

The observed arrival times $\tau_j^{(o)}$, $j = 1,2,\dots,J$ are allowed to associate with the model arrival times $\tau_{i,k}$ corresponding to the discrete model state $\vec{\vartheta}_k$ if their time difference is smaller than the tolerance ε_i. Accordingly an association set can be built for each model peak and each discrete model state

$$\Im(i,k) = \left\{ j \in \{1,2,\dots,J\} : \left|\tau_{i,k} - \tau_j^{(o)}\right| < \varepsilon_i \right\}$$

describing the observed peaks that can be identified by the particular model peak and model state. Since the search windows may overlap with each other, the sets $\Im(i,k)$ may also be partially or totally overlapping with each other.

The matching index $M(k)$, i.e. the number of peaks that a particular model state $\vec{\vartheta}_k$ can explain (identify), can be obtained through successive inspection of all association sets and assignment of the first available (i.e. not already assigned) observed peak in each set to the corresponding model peak. In the matched-peak approach, the model states with the largest matching indices, i.e. interpreting the maximum number of observed peaks, are considered as the more likely parametric descriptions of the reception.

$$Q = \left\{ \hat{k} : M(\hat{k}) = \max\left(M(k)\right) \right\}$$

In this way the solution to the inverse problem is a population Q of model states rather than a single model state.

In the case of multiple receivers $n = 1,2,\dots,N$ with observed arrival times $\tau_{j,n}^{(o)}$, $j = 1,2,\dots,J(n)$ and theoretical arrivals $\tau_{i,n,k}$, $i = 1,2,\dots,I(n,k)$ corresponding to the discrete model state $\vec{\vartheta}_k$ the above associations can be applied to each receiver, resulting in a matching index $M_n(k)$ for each hydrophone. The cumulative matching index is then defined as

$$\mathbf{M}(k) = \frac{1}{N}\sum_{n=1}^{N}\frac{M_n(k)}{J(n)}$$

The matching index for each receiver is normalized by the number of observed arrivals such that equal weight is given to each hydrophone. Further the cumulative matching index $\mathbf{M}(k)$ is normalized by the number of receiving hydrophones such that it ranges between 0 and 1. The number of receiving hydrophones may in general be different from reception to reception.

In the case of multiple receivers, small changes in the model state may drastically change the matching index at particular hydrophones, resulting in a small number of discrete model states achieving the maximum value of the cumulative matching index. In this connection, and in order to increase the robustness of the inversion results, the population of selected model states is built not only from the model states reaching the maximum value of the cumulative matching index, but also from model states above a certain threshold.

$$Q = \left\{ \hat{k} : \mathbf{M}(\hat{k}) > q \cdot \max\left(\mathbf{M}(k)\right) \right\}$$

The threshold is related to the maximum value of $\mathbf{M}$. The tolerance parameter q is taken between 0.8 and 0.9.

5   MCMC sampling

As an alternative to exhaustive grid search of the parameter domain Θ for the model states with maximum cumulative matching index $\mathbf{M}$, a Markov Chain Monte Carlo (MCMC) approach is used to selectively sample the areas characterized by high values of the matching index. The MCMC is known as a method which, starting with a probability density function (pdf), generates a population which asymptotically follows that pdf. This means that the created population is more dense in those areas of the domain of definition of the random variable (or random vector) where the pdf attains its maxima. The population is generated with the Metropolis-Hastings algorithm briefly presented below.

Assume that $\vec{\vartheta}$ is a random vector following the distribution $p(\vec{\vartheta})$. The Metropolis-Hastings algorithm creates a population $\{\vec{\vartheta}_m\}$ of realizations of $\vec{\vartheta}$ (Markov chain) whose histogram asymptotically follows $p(\vec{\vartheta})$. Starting with an arbitrary value of $\vec{\vartheta}$, say $\vec{\vartheta}_1$, a new candidate value for $\vec{\vartheta}$, say $\vec{\vartheta}_{2,C}$, is drawn by using a proposal pdf $q(\vec{\vartheta}; \vec{\vartheta}_1)$ which depends only on $\vec{\vartheta}_1$. The proposal pdf may be arbitrary (e.g. a Gaussian or uniform pdf centered at $\vec{\vartheta}_1$). The candidate value $\vec{\vartheta}_{2,C}$ is now subjected to an acceptance test; if it passes the test then it becomes the second member of the population ($\vec{\vartheta}_2 \leftarrow \vec{\vartheta}_{2,C}$), otherwise the second member of the population is set to be identical to the first member

$(\vec{\mathcal{G}}_2 \leftarrow \vec{\mathcal{G}}_1)$. These steps are repeated in the second round: starting with $\vec{\mathcal{G}}_2$ a new candidate $\vec{\mathcal{G}}_{3,C}$ is picked by using the proposal pdf $q(\vec{\mathcal{G}}; \vec{\mathcal{G}}_2)$, depending now on $\vec{\mathcal{G}}_2$. The new candidate undergoes the acceptance test for becoming the third member of the population or not, and so on. Given the population member $\vec{\mathcal{G}}_\lambda$ and the candidate value $\vec{\mathcal{G}}_{\lambda+1,C}$ for the next population member, the acceptance test is as follows

$$\vec{\mathcal{G}}_{\lambda+1} \leftarrow \begin{cases} \vec{\mathcal{G}}_{\lambda+1,C} & \text{if} \quad a > \xi \\ \vec{\mathcal{G}}_\lambda & \text{if} \quad a < \xi \end{cases}$$

where

$$a = \min\left\{1, \frac{p(\vec{\mathcal{G}}_{\lambda+1,C}) \, q(\vec{\mathcal{G}}_\lambda; \vec{\mathcal{G}}_{\lambda+1,C})}{p(\vec{\mathcal{G}}_\lambda) \, q(\vec{\mathcal{G}}_{\lambda+1,C}; \vec{\mathcal{G}}_\lambda)}\right\}$$

and ξ is a random number between 0 and 1 following the uniform distribution, $\xi \sim U[0,1]$.

This means that the candidate value $\vec{\mathcal{G}}_{\lambda+1,C}$ is accepted with probability a. For the calculation of a the pdf f needs to be evaluated at $\vec{\mathcal{G}}_\lambda$ and $\vec{\mathcal{G}}_{\lambda+1,C}$; furthermore the proposal pdf needs to be evaluated at $\vec{\mathcal{G}}_{\lambda+1,C}$ given $\vec{\mathcal{G}}_\lambda$ and reciprocally at $\vec{\mathcal{G}}_\lambda$ given $\vec{\mathcal{G}}_{\lambda+1,C}$.

In the case of selective sampling of the parameter domain Θ in search of model states with maximum cumulative matching index, the function $\mathbf{M}(\vec{\mathcal{G}})$ plays the role of the distribution. In order to amplify the maxima of $\mathbf{M}(\vec{\mathcal{G}})$ and thus constrain the generated population as close to the maxima as possible a power of the cumulative matching index can be taken $f(\vec{\mathcal{G}}) \propto \mathbf{M}^\beta(\vec{\mathcal{G}})$.

6   The tomography data

Fig. 4 presents the travel-time data at the 8 receiving hydrophones during the 10 months of the Fram-Strait tomography experiment after mooring-motion and clock-drift correction. In particular for each reception the 40 highest peaks are picked and their amplitude is represented by the color scale. Each of the plots corresponds to a particular hydrophone, from the uppermost (top) to the lowermost (bottom). Due to a problem in the upper STAR unit the receptions at the upper 4 hydrophones are sparser than the ones at the lower 4. Still, even at the lower 4 hydrophones there are periods (up to several days) of no data. This means that inversions on different days must rely on a different number of receivers, depending on data availability. The maximum peaks (in read) in Fig. 4 correspond mostly to waterborne acoustic arrivals whereas the lower ones (green and yellow) correspond to noise.
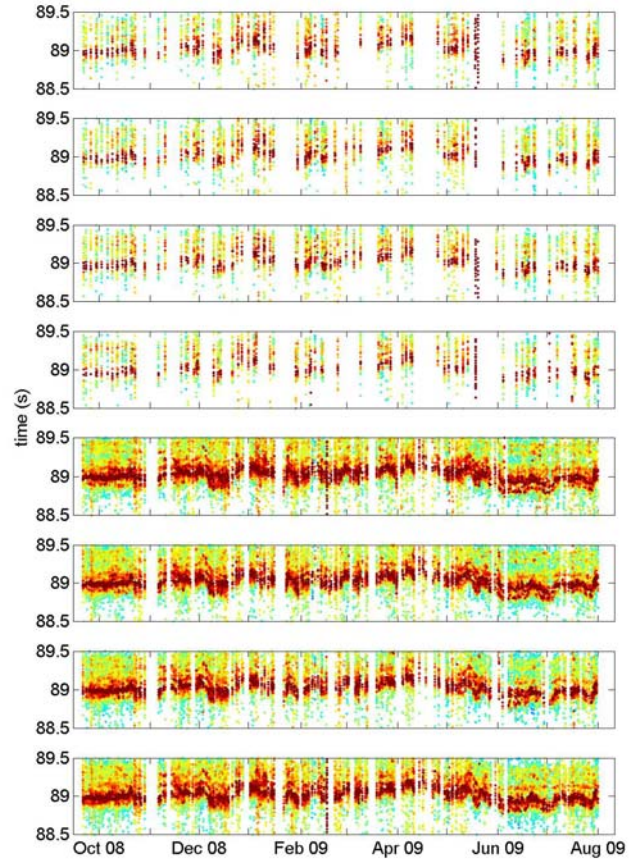

Fig. 4. Travel-time data at the 8 receiving hydrophones. Arrival amplitudes are represented by the color scale (red: highest).

The travel-time data resulting from daily coherent averaging of the arrival patterns and noise filtering are shown in Fig. 5. Similar remarks apply here as in Fig. 4 concerning the data quality. The small variability in depth of the temperature (sound speed) in the area limits the waterborne arrival pattern to about 200 msec. Tracks of individual peaks can hardly be seen. Furthermore, there are hardly any signs of bottom reflected arrivals which means that these arrivals are hidden in the background noise.

7   Inversion results

For the inversion of the measured travel-time data the matched-peak approach with MCMC sampling is applied.

The first 5 EOFs are used for the parameterization of the temperature (sound-speed) distribution. The parameter domain corresponding to the 5 EOF amplitudes is set to ± 3 times the corresponding rms EOF amplitude. Further the proposal distribution is taken uniform over the interval ± 1.5-2 times the rms EOF amplitude. The number of samples in the MCMC was set to 20000 (repetition of the analyses with 40000 samples has given very similar
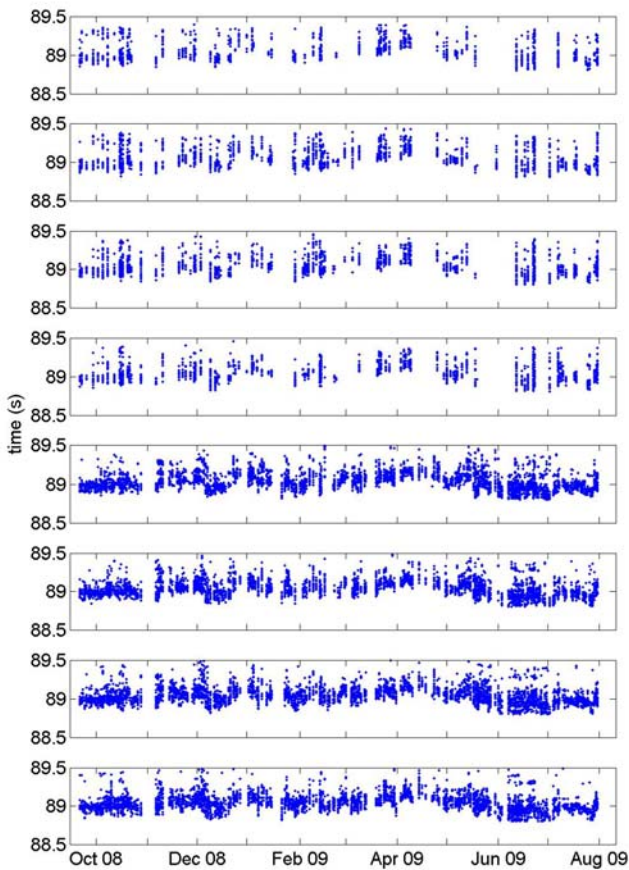
Fig. 5. Travel-time data at the 8 receiving hydrophones after daily coherent averaging and noise filtering.

results). For peak matching the tolerance ε is set to 5 msec and the threshold parameter q to 0.8, i.e. the population of selected model states is those resulting in a cumulative matching index larger that 80% of the maximum matching index.

Fig. 6 shows the distribution of the amplitudes of the 5 EOFs corresponding to the population of selected model states resulting from the inversion. In most cases the distributions are well within the allowed variability intervals (±3 times the rms amplitudes).

Fig. 7 shows the reconstructed travel times (red dots) for the 8 hydrophones, i.e. the travel times predicted for the model states corresponding to the mean EOF amplitudes. The observed travel times are also shown as black dots for comparison. It is seen that the theoretical travel times sufficiently represent the measured travel times.

Fig. 8 shows the heat content evolution represented by the temperature average between the surface and the depth of 2000 m resulting from the inversion of the travel-time data over the 10-month duration of the experiment. The error bars represent the rms variability of the selected population of model states for each reception. The average

temperature from the KV Svalbard (KVS) and Håkon Mosby (HM) oceanographic surveys along the tomographic section, also shown in the figure, are in agreement with the inversion results. The Håkon Mosby (recovery cruise) data are from 5-6 August 2009, i.e. a week after the end of the transmissions. From the temperature evolution it is seen that there is a general cooling during winter which is interrupted by shorter-term warming episodes.
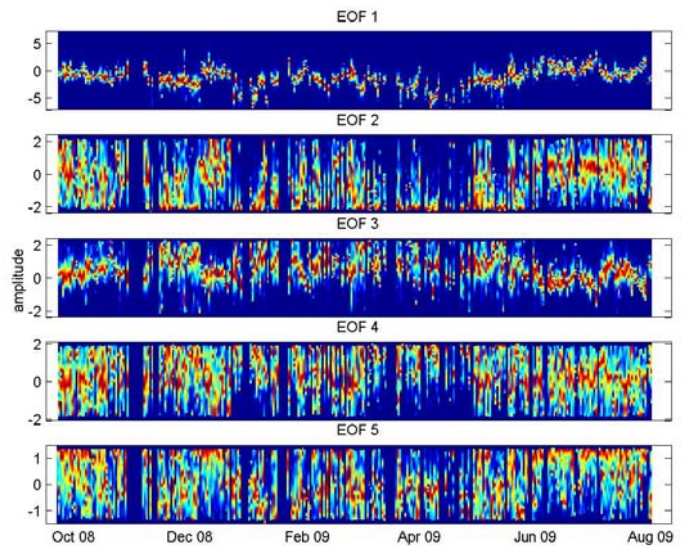

Fig. 6. Distribution of EOF amplitudes.

Fig. 9 shows the evolution of the average temperature in the 150-500-m layer. This layer is the most important one in the area since it represents the Atlantic water. Previous inversion studies [6] have shown that, due to the particular propagation conditions in the Fram Strait area, ocean acoustic tomography has maximum resolution in that layer. The 150-500-m average temperature from the KV Svalbard (KVS) and Håkon Mosby (HM) surveys are in agreement with the inversion results.

The temperature evolution in the 150-500-m layer has a similar behavior as in the 0-2000-m layer: general cooling during winter interrupted by short term warming episodes. The latter are attributed to mesoscale activity in the area of the Return Atlantic current.

It will be interesting to compare these results with the data from the AWI moored array (78°50′N) for the period summer 2008 – summer 1010 that will be recovered in July 2010.
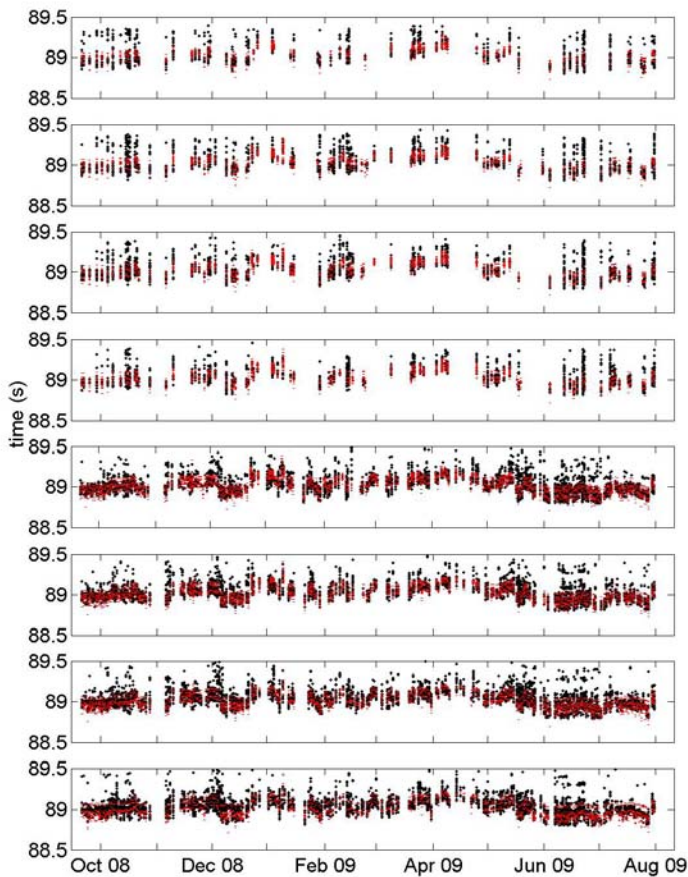
Acknowledgements

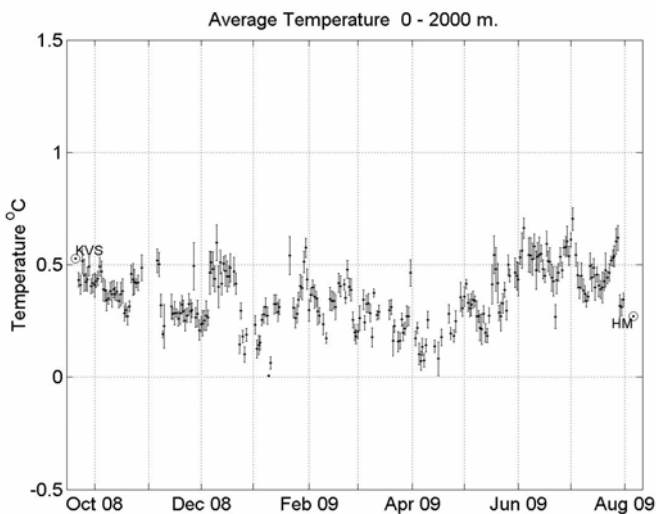Fig. 7. Theoretical (red) and observed (black) travel times at the 8 hydrophones.

Fig. 8. Evolution of range-average temperature over 0-2000-m layer (entire water column) resulting from inversion and comparison with KV Svalbard (KVS) and Håkon Mosby (HM) data.
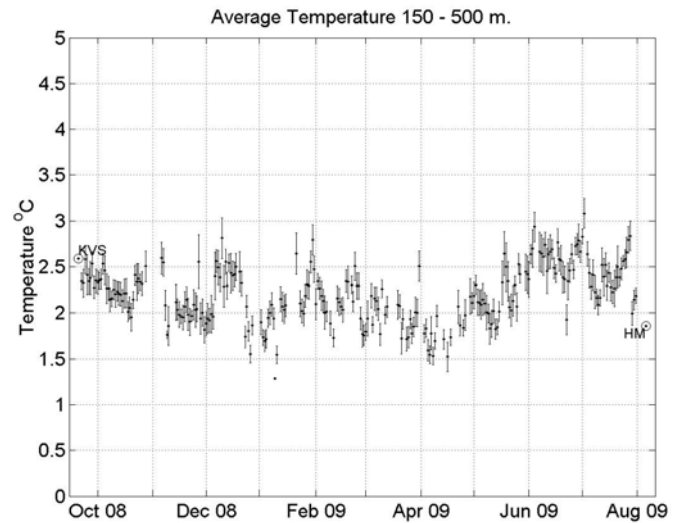

Fig. 9. Evolution of range-average temperature over 150-500-m layer (Atlantic water layer) resulting from inversion and comparison with KV Svalbard (KVS) and Håkon Mosby (HM) data.

References

[1] Schauer, U., Beszczynska-Möller, A., Walczowski, W., Fahrbach, E., Piechura, J., Hansen, E..Variation of Measured Heat Flow Through the Fram Strait Between 1997 and 2006,, in Arctic-Subarctic Ocean Fluxes: Defining the Role of the Northern Seas in Climate, R. Dickson et al. (Ed.), Springer, 65-85, (2008).

[2] Sagen H., S. Sandven, P. Worcester, M. Dzieciuch and E. Skarsoulis, The Fram Strait acoustic tomography system, Proc. 9th Eur. Conf. on Underwater Acoustics, Paris, 13-18, (2008).

[3] Sandven, S., H. Sagen, S.A. Haugen, J. Wåhlin, S.L. Johansen, S. Myking, P. Worcester, A. Morozov, C. Hubbard, A. Smerdon, J. Abrahamsen, K. Bruserud, J. Johansen, P. Wieczorek, A. Beszczynska-Moeller, O. Strothmann, H. Legoff, H. Hobæk, and V. Rosello, The Fram strait tomography experiment 2008, NERSC Technical report No. 298 (2008).

[4] Chen C-T. and F.J. Millero, Speed of sound in seawater at high pressures, *J. Acoust. Soc. Am.*, 62, 1129-1135 (1977).

[5] Skarsoulis, E.K., A matched-peak inversion approach for ocean acoustic travel-time tomography, *J. Acoust. Soc. Am.*, 107, 1324-1332 (2000).

[6] Skarsoulis E., G. Piperakis, M. Kalogerakis, H. Sagen, Ocean acoustic tomography: Travel-time inversions in the Eastern Fram Strait, Proc. 9th Eur. Conf. on Underwater Acoustics, Paris, 19-23 (2008).